Changes in satellite retrievals of atmospheric composition over eastern China during the 2020 COVID-19 lockdowns

Robert D. Field[1,2], Jonathan E. Hickman[1], Igor V. Geogdzhayev[1,2], Kostas Tsigaridis[1,3], Susanne E. Bauer[1]

[1]NASA Goddard Institute for Space Studies, 2880 Broadway, New York, NY, USA, 10025
[2]Dept. of Applied Physics and Applied Mathematics, Columbia University 2880 Broadway, New York, NY, USA, 10025
[3]Center for Climate Systems Research, Columbia University, 2880 Broadway, New York, NY, USA, 10025

Correspondence to: Robert D. Field (robert.field@columbia.edu)

Abstract. We examined daily Level-3 satellite retrievals of AIRS CO, OMI SO_2 and NO_2, and MODIS AOD over eastern China to understand how COVID-19 lockdowns affected atmospheric composition, taking into account trends that have occurred since 2005. Over central east China during the January 23 - April 8 lockdown window, CO in 2020 was 12% lower than the 2005-2019 mean, but only 2% lower than what would be expected given the decreasing CO trend over that period. Similarly for AOD, 2020 was 30% lower than the 2011-2019 mean, but not distinct from what would be expected from the trend. NO_2 in 2020 was 43% lower than the 2011-2019 mean, but only 17% lower than what would be expected given the trend over that period. Over southern China, 2020 NO_2 was not significantly different from anticipated, and CO and AOD were significantly higher that what would be expected, which we suggest was partly because of an active fire season in neighbouring countries. Over east central and southern China, SO_2 was higher than expected, but the magnitude depended strongly on how daily regional values were calculated from individual retrievals. Future work over China, or other regions, needs to take these trends into account in order to separate the effects of COVID-19 on air quality from recent trends, or from variability in other sources.

1 Introduction

In an effort to control the spread of COVID-19, the Chinese government implemented a range of restrictions on movement. These led to reductions in industrial and other work related and personal activities starting January 23, 2020 in Wuhan, Hubei province, then extending to other cities and regions in the days that followed. On April 8, 2020, Wuhan was the last city to re-open after a complete lockdown that prevented most people from leaving their homes. These measures have been linked to changes in air quality. A network of surface monitoring stations in northern China observed 35% decreases in $PM_{2.5}$ and 60% decreases in NO_2 concentrations during January 29 through February 29, as compared to the preceding three weeks; CO and SO_2 also declined (Shi and Brasseur, 2020). In and around Wuhan, decreases of NO_2 and $PM_{2.5}$ were similar to regional changes, but there was a slight increase in SO_2 concentrations (Shi and Brasseur, 2020). Observations by the Tropospheric Monitoring Instrument (TROPOMI) showed large decreases in tropospheric NO_2 column densities over Chinese cities, on the order of 40% for February 11 to March 24 2020 compared to the same period in 2019, ranging from roughly 25% for cities not affected by lockdown to 60% for Wuhan and Xi'an (Bauwens et al., 2020). Prospective simulations suggested that meteorology may limit the effect of reduced emissions on $PM_{2.5}$ concentrations, with Chinese cities experiencing less than 20% reductions (Wang et al., 2020).

The goal of our study was to consider these changes against pollution trends in China using NASA Earth Observing System data by combining several products to give a holistic view covering several emission sectors that are responsible for the observed changes. Over the last 2 to 3 decades, air pollution in China appears to have followed the pattern described by the Environmental Kuznets Curve (Selden and Song, 1994). This framework describes a relationship in which economic growth is initially accompanied by an increase in air pollution, when poverty remains widespread. But as growth continues, air pollution is expected to level off and decline as a consequence of changes in social awareness of environmental degradation and the economic, political, and technological capacity to limit it (Sarkodie and Strezov, 2019;Selden and Song, 1994).

Bottom-up and top-down assessments of air pollutant emissions and concentrations suggest that China has followed this pattern during the era of satellite monitoring of atmospheric composition, with concentrations of SO_2, NO_2, CO, and aerosol optical depth (AOD) mostly exhibiting marked and steady declines over the last decade. In the case of NO_2, multi-instrument analyses, which extend the observational record beyond the lifetime of a single instrument, depict a consistent regional picture of NO_2 trends in China since 1996 (Geddes et al., 2016;Georgoulias et al., 2019;Wang and Wang, 2020;Xu et al., 2020). Column totals show an increasing trend during the first part of the satellite record, but this trend is reversed sometime between 2010 and 2014 (Georgoulias et al., 2019;Krotkov et al., 2016;Lin et al., 2019;Xu et al., 2020;Si et al., 2019;Shah et al., 2020). The trend reversal has been attributed to a combination of emission control measures (Zheng et al., 2018a) and variations in economic growth (Krotkov et al., 2016).

Bottom-up estimates suggest that SO_2 emissions peaked earlier, with declines starting around 2005, primarily as a result of power and industrial pollution control measures as well as the elimination of small industrial boilers (Sun et al., 2018;Zheng et al., 2018b). An earlier peak in SO_2 emissions is consistent with observations by multiple satellite instruments, which revealed declines in SO_2 column densities since 2005 (Fioletov et al., 2016;Krotkov et al., 2016;Wang and Wang, 2020;Zhang et al., 2017;Si et al., 2019).

AOD retrievals from the Along Track Scanning Radiometer instruments show a steady increase over southeastern China from 1995 to 2005 (Sogacheva et al., 2020), and a decline since 2005 in the MODIS AOD (He et al., 2019). The AOD peak has been argued to match either the ~2011 peak in NO_2 (Zheng et al., 2018b;Xie et al., 2019), the ~2005 peak of SO_2, or to have occurred at some point in between (Ma et al., 2016), with more rapid decreases in AOD after 2011 (Lin et al., 2018). The recent decrease in AOD is also seen in VIIRS retrievals (Sogacheva et al., 2020). Most mitigation of direct $PM_{2.5}$ emissions since 2010 was by industry, with residential emissions also decreasing substantially (Zheng et al., 2018b). The decline in SO_2 emissions also exerted an important influence, with the sulfate concentration of $PM_{2.5}$ decreasing substantially between 2013 and 2017 (Shao et al., 2018), reflecting the negative trend in SO_2 emissions.

The peak in concentrations of CO, which has an atmospheric lifetime ranging from weeks to months, is less easily identified. Some studies suggest that trends have been negative potentially throughout the 21st century (Han et al., 2018;Strode et al., 2016;Wang et al., 2018;Yumimoto et al., 2014;Zheng et al., 2018a), but others suggest that

emissions and/or column densities were increasing or flat during at least the first decade of the century (Sun et al., 2018;Zhao et al., 2013;Zhao et al., 2012). The negative trend has been attributed largely to reductions in emissions from industrial activity, as well as from residential and transportation sectors (Zheng et al., 2018a;Zheng et al., 2018b).

In addition to these long-term trends, a number of air pollutants also exhibit strong seasonal variation in China. Anthropogenic emissions of CO, SO_2, and $PM_{2.5}$ are highest in winter, reflecting large variation in emissions from the residential sector and, in the case of CO, increased emissions associated with cold-start processes in the transportation sector (Li et al., 2017). Outflow of CO and AOD has a spring maximum, resulting from transport of pollution, dust, and boreal biomass burning emissions (Han et al., 2018;Luan and Jaegle, 2013).

Changes in pollution over China have also come from short-term interventions. To improve air quality for the 2008 summer Olympics—a time when emissions in China were high and still increasing—the Chinese government imposed a series of strict emissions control measures from July through September 21, 2008, which were qualitatively similar to the emissions reductions expected to have accompanied the COVID-19 lockdown (UNEP, 2009). As a result, NO_2 concentrations over Beijing were estimated to have declined by between 40% and 60% based on satellite observations, with substantial but smaller reductions in surrounding cities often on the order of 20% to 30% compared to previous years (Mijling et al., 2009;Witte et al., 2009). Regional reductions of SO_2 and CO during the months of the games were estimated to be 13% and 19%, respectively (Witte et al., 2009). These results are broadly consistent with on-road observations (Wang et al., 2009), but larger than some surface observations comparing concentrations before and after the emission control measures were implemented (Wang et al., 2010).

The COVID-related lockdowns provide a similar natural experiment to the 2008 Beijing Olympics but on the other side of the Kuznets curve. The fact that the lockdowns occurred during years of decreasing air pollution needs to be taken into account in attributing changes in atmospheric composition to COVID-19 lockdowns, independent of the long-term trend. Following Chen et al.'s (2020) analysis of air quality improvements on mortality which controlled for changes in air quality since 2016, in this study we determine whether changes in 2020 in satellite retrievals of CO, SO_2, NO_2 and AOD departed significantly from the expected declines associated with the long-term decreases in concentrations resulting from pollution controls and technological change.

2 Data and methods

We used daily Level-3 (L3) retrievals from four different instruments on three different NASA Earth Observing System satellites. The Atmospheric Infrared Sounder (AIRS) instrument aboard NASA's Aqua satellite is a 2300-channel infrared grating spectrometer in a sun-synchronous orbit with northward equator crossing time of 1:30 PM. AIRS carbon monoxide (CO) profiles are retrieved with horizontal resolution of 45 km at nadir, in a swath of width 30 fields-of-view or about 1600 km. The retrieval uses a cloud-clearing methodology providing CO with sensitivity that peaks around 500 hPa, with ~0.8-1.2 degrees-of-freedom-of-signal for 50-70% of scenes. More sampling and higher information content is obtained in clear scenes (Warner et al., 2013). We used the daily version 6 (AIRS3STD.006) product.

The Ozone Monitoring Instrument (OMI) aboard NASA's Aura satellite was launched in July 2004, and has a local equator-crossing time of roughly 13:45. OMI is a nadir-viewing spectrometer, which measures solar backscatter in the UV-visible range (Krotkov, 2013). We used NASA's L3 tropospheric NO_2 column density Standard Product v3 (OMNO2d_003), and the OMI Principle Components Analysis Planetary Boundary Layer (PBL) SO_2 product (OMSO2e_003), which grid retrievals to 0.25° resolution (Krotkov et al., 2017;Li et al., 2013). Both products are cloud-screened; only pixels that are at least 70% cloud-free are included in the NO_2 product, and those that are at least 80% cloud-free are included in the SO_2 product. The NO_2 product relies on air mass factors (AMFs) calculated with the assistance of an atmospheric chemical transport model and are sensitive to model representations of emission, chemistry, and transport data. Instead of AMFs, the SO_2 product uses spectrally-dependent SO_2 Jacobians, but can be interpreted as having a fixed AMF that is representative of summertime conditions. We applied basic transient SO_2 plume filtering, excluding retrievals with $SO_2 > 15$ DU (Wang and Wang, 2020).

Because our trend analysis uses a seasonal mean as the response variable, we assume that random errors cancel out, leaving only systematic errors, which do not contribute to uncertainty in the trend analysis. Systematic errors in the OMI NO_2 product have an uncertainty of 20% (McLinden et al., 2014) and are associated with AMFs and tropospheric vertical column contents. The OMI NO_2 products use an implicit aerosol correction to account for the optical effects of aerosols, but retrievals can be biased when aerosol loading is extreme (Castellanos et al., 2015). Under these conditions, the OMI NO_2 retrieval is biased low by roughly 20 to 40% (Chimot et al., 2016). Note that any aerosol-related error would have the potential effect of underestimating the magnitude of decreases in NO_2 column densities when comparing 2020 to previous years. Additional bias in the NO_2 product may be introduced due to the reliance on nearly cloud-free pixels, in which greater sunlight may induce higher photochemical rates. For example, the current NO_2 product is biased roughly 30% low over the Canadian oil sands (McLinden et al., 2014). The level-2 OMI- NO_2 product has been validated against in situ and surface-based observations showing good agreement (Lamsal et al., 2014). The use of fixed Jacobians in the SO_2 product introduces systematic errors of 50 to 100% for cloud-free observations (Krotkov et al., 2016).

Starting in 2007, the quality of level 1B radiance data for some OMI viewing directions has been affected, known as the row anomaly. The L3 products used here exclude all pixels affected by the row anomaly from each observation, but the locations of the row anomaly pixels were dynamic between 2007 and 2011, which could affect any comparisons including those years. Since 2011, the pixels affected by the row anomaly problem are the same, so comparisons for data only since 2011 are not affected by changes in the row anomaly.

Moderate Resolution Imaging Spectroradiometer (MODIS) sensors observe the Earth from polar orbit, from Terra satellite since 2000 and from Aqua since mid 2002. In this study we use MODIS-derived AOD at 550nm obtained by merging Dark Target and Deep Blue retrievals (Sayer et al., 2014). Specifically, we use the Deep_Blue_Aerosol_Optical_Depth_550_Land_Mean field over land and the over ocean AOD_550_Dark_Target_Deep_Blue_Combined_Mean the from Collection 6.1 L3 Gridded products MYD08 and MOD08 (Hubanks et al., 2019), though very few retrievals over ocean are included in our analysis. L3 values are

computed on 1° × 1° spatial grid from L2 AOD products with resolution of 10x10 km. Over land 66% of MODIS-retrieved Dark-target AOD values were shown to be ±0.05±.15*AOD AERONET-observed values, with high correlation (R = 0.9) (Levy et al., 2010). Around 78% of the Deep Blue retrievals are within the expected error range of ±0.05±0.20*AOD (Sayer et al., 2013). MODIS AOD data have been extensively used by the modeling and remote sensing scientific communities and inter-compared with a wide range of satellite AOD products (see Schutgens et al. (2020) and references therein).

We analyzed these retrievals over two large regions (Fig. 1). Central east China was comprised of Shaanxi, Hubei, Anhui, Jiangsu, Shanxi, Henan, Hebei, Shandong, Beijing, and Tianjin provinces. Southern China was comprised of Guizhou, Guangxi, Hunan, Jiangxi, Guangdong, Fujian and Zhejiang provinces. Daily mean quantities were calculated across all valid retrievals falling within the provinces comprising the regions. For the OMI NO_2 columns, individual retrievals were weighted by the L3 'Weight' field, which is proportional to the fraction of the grid cell with higher-quality retrievals, identified as those have less than 30% cloud fraction and not affected by the row anomaly problem. We also calculated the daily value from the median of all retrievals, to understand whether individual high values (mainly SO_2) had any effect on the significance of trends or differences between 2020 and different background periods. Monthly averages were calculated from the daily regional averages, with each day weighted in the monthly average by the number of valid retrievals so as to not overrepresent days with little satellite coverage or significant cloud cover. The monthly data were used to visually identify COVID-19 related changes against background seasonality and trends since 2005.

We examined the difference in the distribution of daily data during the 2020 January 23 to April 8 lockdown period to the same period during previous years since 2005. We compared 2020 to 2019, to background periods ending in 2019 over which trends were consistent, and to the expected value for 2020 estimated from these trends. We tested the significance of these differences using bootstrap resampling (Efron and Gong, 1983) with a resampling size of 2000. Given the uncertainty and uneven nature of trends over different parts of China from previous studies, we identified the start of existing long-term trends for each species by conducting linear regressions of the change in the four quantities over time for possible start years of 2005 to 2015. Each trend was estimated from the start year in this range until 2019. We selected the start year for the most significant trend and used that trend for comparisons to 2020 data.

We also considered how the analysis depended on how the lockdown period was defined. Emissions and pollution can decrease during the Chinese New Year holidays (Chen et al., 2020), which started as early as January 23 in 2012 and as late as February 19 in 2015, complicating COVID-19 related analyses of atmospheric composition over China (Bauwens et al., 2020;Chen et al., 2020). The timing and extent of lockdowns also varied between provinces and we assume that 'slowdowns' could have happened before or after stricter, official lockdowns. For example, ground and air transportation remaining below lockdown levels nationally at least through April 14, 2020 (International Energy Agency, 2020). Excluding the holiday period from all years is a straightforward approach to excluding any New Year holiday effects but will exclude simultaneous lockdown effects during the initial, and presumably most strict, stages of the lockdown. Rather than specifying different combinations of New Year holiday period and provincial-level lockdown timing, we used January 23-April 8 as our baseline period

(which will include all holiday periods since 2005), but examined the sensitivity of the statistics to the length of the lockdown period, namely a longer lockdown period beginning one week earlier and one week later, and a shorter lockdown period for February only. In interpreting the data, we put more confidence in 2020 differences that were insensitive to these choices.

3 Results

3.1 Regional patterns and seasonality

Figure 2 shows the 2020 –2019 differences over China during the January 23-April 8 lockdown period for the four satellite-retrieved quantities. There were decreases of 5-10 ppbv in AIRS CO over central east China (Fig. 2a) and increases of 20-25 ppbv over southern China in 2020 compared to 2019. The increase in southern China is adjacent to a stronger positive CO anomaly over the upper Mekong regions of Myanmar, Thailand and Laos. There were no coherent regional changes in OMI SO_2 (Fig. 2b), but rather smaller localized difference of either sign. There were decreases in NO_2 (Fig. 2c) across central east China exceeding $8x10^{15}$ molec cm^{-2} coincident with the weaker decrease in CO. Over southern China, there were comparable differences over Guangdong province, with smaller differences elsewhere. There was a decrease in MODIS AOD (Fig. 2d) in central-east China coincident with the decreases in CO and NO_2, but smaller in magnitude. There was a region of higher AOD in and northeast of the upper Mekong region coincident with the CO increase, both presumably because of biomass burning.

To put the 2020/2019 difference maps in a longer-term and seasonal context, Figure 3 shows monthly averages of the four retrieved quantities over central east China since 2005. There are seasonal CO peaks in March-April, June and September, with the minima usually in November and December (Figure 3a). There has been a decrease since 2005 in CO. The seasonal decrease from January to February in 2020 is similar to that which has occurred occasionally before, but the CO during February and March 2020 was the lowest for that time of the year since 2005. By April, CO had returned to levels typical of 2015-2019. The main characteristics of the monthly SO_2 over the region are that it has decreased since 2005 (Figure 3b), and that early 2020 SO_2 was within the range of recent levels. There is a strong seasonal NO_2 cycle (Figure 3c), with a July-August minimum, and December-January peak, which has been attributed to increased heating needs (Yu et al., 2017;Si et al., 2019) and longer chemical lifetime owing to lower OH and RO_2 (Shah et al., 2020). NO_2 has also decreased since 2011, and during most years, there is a departure from a smooth seasonal cycle in January and February associated with the Chinese New Year holiday period. January and February 2020 NO_2 was considerably lower than previous years, increased during March, and had recovered to typical, recent levels by April. AOD has consistent seasonal peaks in summer which have been attributed to hygroscopic growth and agricultural residue burning (Filonchyk et al., 2019), but had less regular seasonality otherwise, and has decreased since 2011. AOD during February and particularly March of 2020 were lower than recent years, but during which time there was considerable variability in the monthly data.

Figure 4 shows the four retrieved quantities over southern China. There is a springtime maximum in CO (Fig. 4a), a less regular maximum during September-January, and an annual minimum in July. The range of CO is similar

to central east China. CO over the last 5 years is lower than earlier in the record, and early 2020 CO was higher than recent years. SO_2 (Fig. 4b) is lower than central east China and any seasonal cycle is also hard to identify. The high June 2011 values are due to the Nabro eruption in Ethiopia (Fromm et al., 2014) which is still apparent in the time series despite excluding individual SO_2 retrievals that are greater than 15 DU, and are due to a combination of higher overall background values and individual retrievals with very high (> 10 DU) SO_2. NO_2 (Fig. 4c) is lower than over east central China, but both regions share a similar seasonality. NO_2 during January-April 2020 was slightly lower than in 2019. AOD (Fig. 4d) has weak seasonal peaks in October, March and June, has decreased since 2011, and 2020 fell within the range of 2015-2019.

3.2 East central China

Figure 5 shows the CO, SO_2, NO_2 and AOD for January 23 – April 8 of each year over east central China as box and whisper plots with the median, interquartile range and 2.5th and 97.5th percentiles over all daily mean data as horizontal lines and the mean shown by the black dot. The associated statistics comparing 2020 and 2019 are provided in Table 1, and comparing 2020 with the period over which the trend is most consistent in Table 2. which was determined from the r^2 of the trends for all starting years between 2005 and 2016. The linear trends in each plot start at the year over which the trend explains most of the variability in the data, which will vary by region and variable. The AIRS CO is shown in Figure 5a. The variation during January 23 – April 8 of each year is due to weather-related factors and observational error. The mean CO of 133.5 ppbv in 2020 was 3% less than the 2019 mean of 137.9 ppbv, and 12% less than 2005-2019 mean of 150.9 ppbv. The 2020 difference from 2019 is only marginally significant, with a 95% confidence interval (-6% - 0%) close to spanning 0. The 2020 difference from the 2005-2019 background is significant (-14% - -9%), but during this period CO declined by -1.8 ppbv yr^{-1}, indicated by the red points. This overall decrease includes periods where CO may have increased, for example from 2010-2012, 2016 and slightly in 2019. Based on this trend, the expected value for 2020 was 136.8 ppbv (shown in blue). The observed 2020 mean was 2% less than expected, but because the 95% confidence intervals (-5% - 1%) span 0, this difference is not considered to be significant. Results were similar for CO analysed closer to the surface at 850 hPa, but where the retrieval has less sensitivity.

OMI SO_2 (Fig. 5b) fluctuated over 2005 to 2011 and declined steadily afterward by -.056 DU yr^{-1} from 2012-2019 over east central China. This trend explained 32% of the variation in the data over this period, during which overall variation declined, becoming narrower to a degree not seen in the CO. Declines were steady, although 2019 may have departed upward from this trend. The 2020 mean of 0.058 was 94% higher than the 2019 mean of 0.031, but with a wide 95% confidence interval (16% - 226%). 2020 SO_2 was 72% lower than the 2012-2019 mean, and with a narrower (-79% - -65%) confidence interval. The observed 2020 SO_2 was 202% higher than the expected value of -0.06; the large percent difference reflects an expected value close to zero, and we note that the retrieved SO_2 can be negative for individual values and averages (Li et al., 2013; Wang and Wang 2020). While this difference was significant, the change in 2020 SO_2 was strongly dependent on whether daily values were calculated from the mean or median of individual values over the region. When the median of individual retrievals is used, 2020 was only 8.4% higher than predicted from the 2012-2019 trend (Figure S1b). This likely reflects the

greater influence of high individual retrieval values on the daily mean value compared to the median, even after the basic filtering of transient SO_2 plumes.

OMI NO_2 (Fig. 5c) increased from 2005 to 2011 and decreased by -0.7x10^{15} molec cm^{-2} yr^{-1} from 2011-2020. The 2020 mean NO_2 of 6.5x10^{15} molec cm^{-2} was 32% less than the 2019 mean of 9.6 x10^{15} molec cm^{-2}, and 43% less than the 2011-2019 mean of 11.3 x10^{15} molec cm^{-2}. The pronounced regional difference between 2020 and 2019 (Fig. 2c) in part likely reflects an upward departure in 2019 from the overall trend since 2011. The observed 2020 mean was 17% less than the expected value of 7.8 x10^{15} molec cm^{-2}, with a wide but negative 95% confidence interval (-28% - -5%), suggesting that 2020 NO_2 was significantly lower than would be expected from the trend.

MODIS AOD (Fig. 5d) was flat or slightly increasing from 2005 to 2011 and subsequently changed by -0.03 yr^{-1}. The 2020 mean AOD of 0.41 was 14% less than the 2019 mean of 0.48 and 29% less than the 2011-2019 average of 0.58. The observed 2020 mean was 2% higher than the predicted value of 0.40, but with a wide (-15% - 20%) confidence interval spanning 0, suggesting 2020 was not significantly different from expected.

In evaluating the 2020 changes, the background period was defined by the period during which the trend was strongest, using the r^2 value of the trend. This is a reasonable but ad-hoc way of defining a period with consistent increasing or decreasing trends. Figure 6 shows how the trends and differences between observed and predicted 2020 means depended on the year chosen as the start of the period over which the trend is estimated, for starting years between 2005 and 2016. AIRS CO (Fig. 6a) showed uneven changes in the trend (red line) with starting year, and more uncertainty in the trend (red shading) for later years due to fewer data used for the estimate, but for all years was significantly negative. The difference between observed 2020 mean and the value predicted from the trend (magenta line) varied inversely with the trend and was always negative, but, except for 2009, had 95% confidence intervals (magenta shading) spanning 0, and therefore were not considered significant. The SO_2 trends (Fig. 6b) were all significantly negative. For trends starting in 2007 and after, the observed 2020 mean was significantly higher than predicted, but these differences were not consistently significant when daily values were calculated from the median of individual retrievals (Figure S2b). Earlier starting years produce weaker overall trends in NO_2 (Fig. 6c) because of the NO_2 increase until 2011, but observed 2020 NO_2 was significantly less than predicted regardless of the starting year. As the NO_2 trend approached 0 for periods beginning after 2012, the 2020 differences from what would be expected increased. For a period beginning in 2016, for example, the 2020 NO_2 was 32.8% less than the mean over this period and 28.9% less than what would be expected from the trend. Note that analyses of SO_2 and NO_2 that include years prior to 2012 may be affected by changes in observation sample size due to changes in the OMI row anomaly. For AOD (Fig. 6d), there was no significant difference between the observed and predicted 2020 mean for periods beginning in 2009 and later, when the trends were strongest, and which approached 0 after 2014.

3.3 Southern China

Figure 7 shows the distribution of daily CO, SO_2, NO_2 and AOD for January 23-April 8 of each year over southern China, along with linear trends. The associated statistics comparing 2020 and 2019 are provided in Table 3, and comparing 2020 with the period over which the trend is consistent in Table 4. For AIRS CO (Fig. 7a), the strongest

trend started in 2016 and was -4.8 ppbv yr^{-1} through 2019. CO in 2020 was 144.9 ppbv, 13% higher than the 2019 mean of 128.4 ppbv which can be seen in an upward shift in the distribution of the box plot, and higher than the 2016-2019 background period mean of 137 ppbv. 2020 CO was 16% higher than predicted from the 2016-2019 trend, and with 95% confidence interval (10% - 23%) not spanning 0.

OMI SO_2 (Fig. 7b) changed by -0.012 DU yr^{-1} beginning in 2007, which is driven by fewer high individual SO_2 values in later years, as in east central China. The 2020 mean of 0.003 DU was 122% higher than the 2019 mean of -0.023 DU with a wide but positive 95% confidence interval (20% - 217%), and 95% less than the 2007-2019 mean of 0.058 DU. The observed 2020 mean was 109% higher than the predicted value of -0.034 DU, with a wide but positive 95% confidence interval (53% - 165%).

OMI NO_2 (Fig. 7c) changed by -0.3 $x10^{15}$ molec cm^{-2} yr^{-1} beginning in 2011. The 2020 mean of $3.3x10^{15}$ molec cm^{-2} was 22% less than 2019 and 32% less than 2011-2019, with both differences significant. The 2020 mean was 7% less than the predicted value of 3.6 $x10^{15}$ molec cm^{-2}, but with a wide 95% confidence interval (-19% - 8%) spanning 0.

MODIS AOD (Fig. 7d) changed by -0.04 yr^{-1} between 2011 and 2019. The 2020 mean AOD of 0.38 was 12% higher than the 2019 mean of 0.34, but with a 95% confidence interval (-6% - 32%) spanning 0. 2020 AOD was 17% less than the 2011-2019 mean of 0.46, but 39% higher than predicted from the trend over this period, and with a wide but positive 95% confidence interval (15% - 68%).

Figure 8 shows the dependence of the trends and 2020 differences from background period to the starting year over southern China. AIRS CO (Fig. 8a) had a significant decreasing trend for all starting years, and regardless of the start year, 2020 was significantly higher than predicted from the trend. SO_2 trends were also negative, and varied similarly to the CO until 2015. The 2020 SO_2 was higher than the background period, but with marginal significance, given that the confidence intervals spanned 0 for later starting years, and because the differences were not significant when daily values were calculated from the median SO_2 of individual retrievals for trends starting in 2008 (Figure S3b) or any other year (Figure S4b). NO_2 trends (Fig. 8c) were more strongly decreasing for periods beginning between 2009 and 2012 and were flat or positive otherwise. The 2020 NO_2 mean was significantly lower than predicted, except for when the trend was estimated beginning in 2011, when it was the strongest. The AOD trends varied similarly to the NO_2 but were significantly negative for all start years until 2015. The 2020 mean was significantly higher than predicted for all starting between 2010 and 2015.

For both regions and all quantities, the differences between observed and predicted values for 2020 were insensitive to a longer lockdown period, or to whether the bootstrap resampling was weighted by the number of valid retrievals each day. For a February-only lockdown period (Figures S5 and S6), the CO trends were more significant when starting in later years, but the differences between the observed and expected values for remained insignificant. The SO_2 trends for different periods were similar. The 2020 SO_2 differences from what would be expected approached 0 for later periods but were also in inconsistent when the median values of individual retrievals were used. Results for NO_2 were unaffected. The AOD 2020 difference from what would be expected

was stronger and technically significant, but still with a very wide confidence interval and therefore difficult to interpret. We emphasize that while a February-only lockdown period is useful for comparison, it is problematic in not including the New Year's holiday periods from all previous years.

4 Discussion and conclusions

The degree to which the COVID-19 lockdowns in China resulted in changes in atmospheric composition depends strongly on whether existing trends are taken into account, and only in certain cases could be considered significant. For AIRS CO over central east China, the 2020 mean was 12% less than that over 2005-2019, but only 2% less than what would be expected given the steady decreases over that period, and this 2% was not significant given the variability of the daily data. Similarly for MODIS AOD, the 2020 mean was 30% less than over 2011-2019, but no different than what would be expected from trends. SO_2 in 2020 was 72% less than over 2012-2019 but was 201% higher than what would be expected from trends. Daily SO_2 calculated from the mean of individual retrievals are sensitive to outlying SO_2 values from transient plumes, and when daily SO_2 was calculated instead from the median across individual retrievals, 2020 SO_2 was only 8% higher than what would be expected, but still significantly.

OMI NO_2 in 2020 over central east China was 43% less than over 2011-2019, but only 17% less than what would be expected from trends. This difference was statistically significant but does suggest that more than half of the reductions in NO_2 in 2020 could be expected independent of COVID-19 lockdowns. For reference, Bauwens et al. (2020) reported a ~40% drop in OMI NO_2 from 2019 to 2020 over cities affected by the lockdown using the QA4ECV retrieval (Boersma et al., 2018), and a ~51% drop in NO_2 over the eight cities (Beijing, Jinan, Nanjing, Qingdao, Tianjin, Wuhan, Xi'an and Zhengzhou) falling within our central east China region. Our analysis cannot be compared directly because we include non-urban areas and define our lockdown period differently, but we can say that a large part of the reduction in that study is likely due to background trends, rather than to COVID-19 lockdowns.

The lack of any significant departure from recent trends in CO and AOD over central east China was unexpected, given its high population density and level of industrial activity. In the case of MODIS AOD, the lack of an observable lockdown effect was possibly due to contributions from other sources unaffected by COVID-19 related lockdowns, limitations in the MODIS AOD retrieval under cloudy conditions, climatological variability from other sources such as mineral dust, and meteorology favourable to secondary aerosol formation which could have offset lower emissions (Wang et al., 2020). The 2020 increase in SO_2 is more difficult to interpret because of the discrepancies between daily values calculated from the mean or median of individual retrievals, but is broadly consistent with surface observations that find no significant change in in-situ surface SO_2 over Wuhan in the daily mean, and a slight increase in daytime SO_2 possibly associated with increased residential heating and cooking (Shi and Brasseur, 2020).

Over southern China, retrieved SO_2, NO_2 and AOD were significantly lower in 2020 compared to recent averages. SO_2 was 95% less than the 2007-2019 mean, but 109% greater than what would be expected from trends. Similarly to central east China, SO_2 was only 5% higher than expected when daily values were calculated from the median

of individual retrievals, rather than the mean. NO_2 in 2020 was 32% less than over 2011-2019, but only 7% less than what would be expected from trends, and this difference was not consistently significant for different trend periods. The more significant reductions in NO_2 in east central China compared to the south is presumably due the former's greater population and industrialization, and consequently higher pollution levels. This is consistent with Chen et al.'s (2020) detection of a larger 2020 decrease in surface NO_2 in Wuhan compared to Shanghai. Retrieved CO in 2020 was nearly identical to the 2007-2019 mean, but 10% higher than what would be expected given the decreasing trend over this period. AOD in 2020 was 17% less than over 2011-2019, but 39% higher than what would be expected from the trend.

The focus of this analysis is on whether satellite retrievals of atmospheric composition over 2020 departed significantly from different background periods and expected values for 2020 when daily variability and trends are accounted for, but it is useful at a preliminary stage to speculate as to how different emissions changes could have contributed to 1) why NO_2 was robustly lower in 2020 over east central China compared to CO and AOD, and 2) why CO and AOD were higher over southern China compared to what would be expected from recent trends.

To understand why NO_2 differences over east central China were more significant than other quantities, Table 5 shows the emissions by sector for a representative set of constituents from the Community Emissions Data System (CEDS) (Hoesly et al., 2018) over China for 2014, the most recent year available. Other bottom-up emissions inventories will vary in absolute emissions amounts and their sector contributions, particularly for more recent periods, but CEDS is the standard available emissions dataset available globally as a baseline for the next IPCC assessment, in anticipation of assessing 2020 COVID-19 related changes to atmospheric composition in other regions, and for modeling studies involving a transboundary transport component. Across all species, energy production, industrial activity, transportation, residential/commercial/other (RCO), and waste disposal constitute the bulk of the emissions. Based on activity data for the first quarter of 2020, energy demand across China declined by 7% compared to 2019, and transportation sector activity declined by 50 to 75% in regions with lockdowns in place (International Energy Agency, 2020). These sectors are direct or indirect sources of numerous pollutants, including SO_2 (the precursor of sulfate aerosol), NO_x, CO, and primary anthropogenic aerosols classified broadly as organic carbon (OC) and black carbon (BC). If we apply the 7% reduction in energy production and mid-point 62.5% reduction to transportation from the IEA, assume a 20% reduction in industrial emissions, 5% reduction in waste emissions, no change in RCO (with commercial decreases offset by residential increases), this yields a 10% reduction in BC, 5% reduction in OC, 14% reduction in SO_2, 14% reduction in CO and 21% reduction in NO_2. The larger reduction in NO_2 relative to other emissions could partly explain why OMI NO_2 column density changes over central east China were stronger than in the other retrievals.

Following Si et al.'s (2019) consideration of biomass burning as a pollution source in China alongside anthropogenic sources, we considered transboundary smoke transport as a possible reason for the higher 2020 CO over southern China, guided by higher CO over the Upper Mekong region in 2020 compared to 2019 (Fig. 2a) and the predominant westerly flow during this time of year (Reid et al., 2013). Table 6 compares January 23-April 8 AIRS CO over southern China to CO emissions estimates from biomass burning from the Global Fire

Assimilation System (GFAS) (Kaiser et al., 2012) over the upper Mekong region (17° N to 25° N, 95° E to 105° E) including parts of eastern Myanmar, northern Thailand, and northern Laos. From 2005 to 2020, variation in GFAS CO over this region explained a moderate (32%) amount of variability in AIRS CO over southern China, suggesting it as is a non-negligible contributor to variation in CO concentration, and a contributor to higher CO in 2020. This illustrates that, at a minimum, sources such as biomass burning smoke and dust that are less affected by COVID-19 related measures will complicate attribution studies. To that end, modeling studies following Wang et al. (2020) will be required to isolate emissions, meteorological and chemical drivers of changes in atmospheric composition and their effects at a process level. With proper instrument-equivalent comparisons, modelling studies will also help to identify the extent to which the lack of significant changes are due to retrieval limitations, namely low sensitivity near the surface where differences would presumably be more pronounced, particularly given remote emissions sources such as dust, biomass burning smoke and volcanic SO_2, which will arrive at higher altitudes.

The key implication of our study is that not taking into account past trends in atmospheric composition will lead to misattribution of changes in air quality to COVID-19 lockdowns, or, at a minimum, that whether differences in 2020 are significant depend on the choice of detrending period and lockdown periods, given its subjectivity. We have approached the issue by comparing data for 2020 to what would have been expected given recent trends and by applying a single lockdown period to two large regions, with additional analyses to gauge the sensitivity of the 2020 differences to these choices. Other studies over China or elsewhere will inevitably use other approaches that more explicitly account for seasonality, meteorology, and which relate changes in pollution over smaller areas (e.g. single provinces or states) to region-specific lockdown measures and timing at a process level. Regardless of the approach, however, it is important to consider recent trends and variability. In places where pollution has decreased, not accounting for recent context will result in over-attribution of changes in pollution to COVID-19. In places where pollution has increased, such as parts of South Asia, this will result in under-attribution.

Code/data availability: All code will be made available if the article is accepted for final publication. All source data are publicly available.

Competing interests: The authors have no competing interests.

Author contribution: All authors conceived of the study. RF, IG and KT conducted the data analysis. RF and JH prepared the manuscript with contributions from all co-authors.

References

Bauwens, M., Compernolle, S., Stavrakou, T., Müller, J., van Gent, J., Eskes, H., Levelt, P. F., van der A., R., Veefkind, J. P., Vlietinck., J., Yu, H., and Zehner, C.: Impact of coronavirus outbreak on NO2 pollution assessed using TROPOMI and OMI observations, Geophysical Research Letters, 2, 0-3, 10.1029/2020GL087978, 2020.

Boersma, K. F., Eskes, H. J., Richter, A., De Smedt, I., Lorente, A., Beirle, S., van Geffen, J., Zara, M., Peters, E., Van Roozendael, M., Wagner, T., Maasakkers, J. D., van der A, R. J., Nightingale, J., De Rudder, A., Irie, H., Pinardi, G., Lambert, J. C., and Compernolle, S. C.: Improving algorithms and uncertainty estimates for satellite NO2 retrievals: results from the quality assurance for the essential climate variables (QA4ECV) project, Atmospheric Measurement Techniques, 11, 6651-6678, 10.5194/amt-11-6651-2018, 2018.

Castellanos, P., Boersma, K. F., Torres, O., and de Haan, J. F.: OMI tropospheric NO2 air mass factors over South America: effects of biomass burning aerosols, Atmospheric Measurement Techniques, 8, 3831-3849, 10.5194/amt-8-3831-2015, 2015.

Chen, K., Wang, M., Huang, C., Kinney, P. L., and Paul, A. T.: Air Pollution Reduction and Mortality Benefit during the COVID-19 Outbreak in China, Lancet Planetary Health, 0-3, 10.1101/2020.03.23.20039842, 2020.

Chimot, J., Vlemmix, T., Veefkind, J. P., de Haan, J. F., and Levelt, P. F.: Impact of aerosols on the OMI tropospheric NO2 retrievals over industrialized regions: how accurate is the aerosol correction of cloud-free scenes via a simple cloud model?, Atmospheric Measurement Techniques, 9, 359-382, 10.5194/amt-9-359-2016, 2016.

Efron, B., and Gong, G.: A Leisurely Look at the Bootstrap, the Jacknife, and Cross-Validation, American Statistician, 37, 36-48, 10.2307/2685844, 1983.

Filonchyk, M., Yan, H. W., and Zhang, Z. R.: Analysis of spatial and temporal variability of aerosol optical depth over China using MODIS combined Dark Target and Deep Blue product, Theoretical and Applied Climatology, 137, 2271-2288, 10.1007/s00704-018-2737-5, 2019.

Fioletov, V. E., McLinden, C. A., Krotkov, N., Li, C., Joiner, J., Theys, N., Carn, S., and Moran, M. D.: A global catalogue of large SO2 sources and emissions derived from the Ozone Monitoring Instrument, Atmospheric Chemistry and Physics, 16, 11497-11519, 10.5194/acp-16-11497-2016, 2016.

Fromm, M., Kablick, G., Nedoluha, G., Carboni, E., Grainger, R., Campbell, J., and Lewis, J.: Correcting the record of volcanic stratospheric aerosol impact: Nabro and Sarychev Peak, Journal of Geophysical Research-Atmospheres, 119, 10.1002/2014jd021507, 2014.

Geddes, J. A., Martin, R. V., Boys, B. L., and van Donkelaar, A.: Long-Term Trends Worldwide in Ambient NO2 Concentrations Inferred from Satellite Observations, Environmental Health Perspectives, 124, 281-289, 10.1289/ehp.1409567, 2016.

Georgoulias, A. K., van der A, R. J., Stammes, P., Boersma, K. F., & Eskes, H. J.: Trends and trend reversal detection in two decades of tropospheric NO2 satellite observations, Atmospheric Chemistry and Physics, 19, 6269–6294, https://doi.org/10.5194/acp-2018-988, 2019.

Han, H., Liu, J., Yuan, H. L., Jiang, F., Zhu, Y., Wu, Y., Wang, T. J., and Zhuang, B. L.: Impacts of Synoptic Weather Patterns and their Persistency on Free Tropospheric Carbon Monoxide Concentrations and Outflow in Eastern China, Journal of Geophysical Research-Atmospheres, 123, 7024-7046, 10.1029/2017jd028172, 2018.

He, Q. Q., Gu, Y. F., and Zhang, M.: Spatiotemporal patterns of aerosol optical depth throughout China from 2003 to 2016, Science of the Total Environment, 653, 23-35, 10.1016/j.scitotenv.2018.10.307, 2019.

Hoesly, R. M., Smith, S. J., Feng, L. Y., Klimont, Z., Janssens-Maenhout, G., Pitkanen, T., Seibert, J. J., Vu, L., Andres, R. J., Bolt, R. M., Bond, T. C., Dawidowski, L., Kholod, N., Kurokawa, J., Li, M., Liu, L., Lu, Z. F., Moura, M. C. P., O'Rourke, P. R., and Zhang, Q.: Historical (1750-2014) anthropogenic emissions of reactive gases and aerosols from the Community Emissions Data System (CEDS), Geoscientific Model Development, 11, 369-408, 10.5194/gmd-11-369-2018, 2018.

Hubanks, P., Platnick, S., King, M., and Ridgway, B.: MODIS Algorithm Theoretical Basis Document No. ATBD-MOD-30 for Level-3 Global Gridded Atmosphere Products (08_D3, 08_E3, 08_M3) and Users Guide (Collection 6.0 & 6.1, Version 4.4, 20 Feb 2019), NASA Goddard Space Flight Center, Greenbelt, MD, 2019.

Kaiser, J. W., Heil, A., Andreae, M. O., Benedetti, A., Chubarova, N., Jones, L., Morcrette, J. J., Razinger, M., Schultz, M. G., Suttie, M., and van der Werf, G. R.: Biomass burning emissions estimated with a global fire assimilation system based on observed fire radiative power, Biogeosciences, 9, 527-554, 10.5194/bg-9-527-2012, 2012.

Krotkov, N. A.: OMI/Aura NO2 Cloud-Screened Total and Tropospheric Column L3 Global Gridded 0.25 degree x 0.25 degree V3, NASA Goddard Space Flight Center, 2013.

Krotkov, N. A., McLinden, C. A., Li, C., Lamsal, L. N., Celarier, E. A., Marchenko, S. V., Swartz, W. H., Bucsela, E. J., Joiner, J., Duncan, B. N., Boersma, K. F., Veefkind, J. P., Levelt, P. F., Fioletov, V. E., Dickerson, R. R., He, H., Lu, Z., and Streets, D. G.: Aura OMI observations of regional SO2 and NO2 pollution changes from 2005 to 2015, Atmospheric Chemistry and Physics, 16, 4605-4629, 10.5194/acp-16-4605-2016, 2016.

Krotkov, N. A., Lamsal, L. N., Celarier, E. A., Swartz, W. H., Marchenko, S. V., Bucsela, E. J., Chan, K. L., Wenig, M., and Zara, M.: The version 3 OMI NO2 standard product, Atmospheric Measurement Techniques, 10, 3133-3149, 10.5194/amt-10-3133-2017, 2017.

Lamsal, L. N., Krotkov, N. A., Celarier, E. A., Swartz, W. H., Pickering, K. E., Bucsela, E. J., Gleason, J. F., Martin, R. V., Philip, S., Irie, H., Cede, A., Herman, J., Weinheimer, A., Szykman, J. J., and Knepp, T. N.: Evaluation of OMI operational standard NO2 column retrievals using in situ and surface-based NO2 observations, Atmospheric Chemistry and Physics, 14, 11587-11609, 10.5194/acp-14-11587-2014, 2014.

Levy, R. C., Remer, L. A., Kleidman, R. G., Mattoo, S., Ichoku, C., Kahn, R., and Eck, T. F.: Global evaluation of the Collection 5 MODIS dark-target aerosol products over land, Atmospheric Chemistry and Physics, 10, 10399-10420, 10.5194/acp-10-10399-2010, 2010.

Li, C., Joiner, J., Krotkov, N. A., and Bhartia, P. K.: A fast and sensitive new satellite SO2 retrieval algorithm based on principal component analysis: Application to the ozone monitoring instrument, Geophysical Research Letters, 40, 6314-6318, 10.1002/2013gl058134, 2013.

Li, M., Zhang, Q., Kurokawa, J., Woo, J. H., He, K. B., Lu, Z. F., Ohara, T., Song, Y., Streets, D. G., Carmichael, G. R., Cheng, Y. F., Hong, C. P., Huo, H., Jiang, X. J., Kang, S. C., Liu, F., Su, H., and Zheng, B.: MIX: a mosaic Asian anthropogenic emission inventory under the international collaboration framework of the MICS-Asia and HTAP, Atmospheric Chemistry and Physics, 17, 935-963, 10.5194/acp-17-935-2017, 2017.

Lin, C. Q., Liu, G., Lau, A. K. H., Li, Y., Li, C. C., Fung, J. C. H., and Lao, X. Q.: High-resolution satellite remote sensing of provincial PM 2.5 trends in China from 2001 to 2015. Atmospheric Environment, 180, 110–116, https://doi.org/10.1016/j.atmosenv.2018.02.045, 2018.

Lin, N., Wang, Y. X., Zhang, Y., and Yang, K.: A large decline of tropospheric NO2 in China observed from space by SNPP OMPS, Science of the Total Environment, 675, 337-342, 10.1016/j.scitotenv.2019.04.090, 2019.

Luan, Y., and Jaegle, L.: Composite study of aerosol export events from East Asia and North America, Atmospheric Chemistry and Physics, 13, 1221-1242, 10.5194/acp-13-1221-2013, 2013.

Ma, Z. W., Hu, X. F., Sayer, A. M., Levy, R., Zhang, Q., Xue, Y. G., Tong, S. L., Bi, J., Huang, L., and Liu, Y.: Satellite-Based Spatiotemporal Trends in PM2.5 Concentrations: China, 2004-2013, Environmental Health Perspectives, 124, 184-192, 10.1289/ehp.1409481, 2016.

McLinden, C. A., Fioletov, V., Boersma, K. F., Kharol, S. K., Krotkov, N., Lamsal, L., Makar, P. A., Martin, R. V., Veefkind, J. P., and Yang, K.: Improved satellite retrievals of NO2 and SO2 over the Canadian oil sands and comparisons with surface measurements, Atmospheric Chemistry and Physics, 14, 3637-3656, 10.5194/acp-14-3637-2014, 2014.

Mijling, B., van der A, R. J., Boersma, K. F., Van Roozendael, M., De Smedt, I., and Kelder, H. M.: Reductions of NO2 detected from space during the 2008 Beijing Olympic Games, Geophysical Research Letters, 36, 10.1029/2009gl038943, 2009.

Reid, J. S., Hyer, E. J., Johnson, R. S., Holben, B. N., Yokelson, R. J., Zhang, J. L., Campbell, J. R., Christopher, S. A., Di Girolamo, L., Giglio, L., Holz, R. E., Kearney, C., Miettinen, J., Reid, E. A., Turk, F. J., Wang, J., Xian, P., Zhao, G. Y., Balasubramanian, R., Chew, B. N., Janjai, S., Lagrosas, N., Lestari, P., Lin, N. H., Mahmud, M., Nguyen, A. X., Norris, B., Oanh, N. T. K., Oo, M., Salinas, S. V., Welton, E. J., and Liew, S. C.: Observing and understanding the Southeast Asian aerosol system by remote sensing: An initial review and analysis for the Seven Southeast Asian Studies (7SEAS) program, Atmospheric Research, 122, 403-468, 10.1016/j.atmosres.2012.06.005, 2013.

Sarkodie, S. A., and Strezov, V.: A review on Environmental Kuznets Curve hypothesis using bibliometric and meta-analysis, Science of the Total Environment, 649, 128-145, 10.1016/j.scitotenv.2018.08.276, 2019.

Sayer, A. M., Hsu, N. C., Bettenhausen, C., and Jeong, M. J.: Validation and uncertainty estimates for MODIS Collection 6 "Deep Blue" aerosol data, Journal of Geophysical Research-Atmospheres, 118, 7864-7872, 10.1002/jgrd.50600, 2013.

Sayer, A. M., Munchak, L. A., Hsu, N. C., Levy, R. C., Bettenhausen, C., and Jeong, M. J.: MODIS Collection 6 aerosol products: Comparison between Aqua's e-Deep Blue, Dark Target, and "merged" data sets, and usage recommendations, Journal of Geophysical Research-Atmospheres, 119, 13965-13989, 10.1002/2014jd022453, 2014.

Schutgens, N., Sayer, A. M., Heckel, A., Hsu, C., Jethva, H., de Leeuw, G., Leonard, P. J. T., Levy, R. C., Lipponen, A., Lyapustin, A., North, P., Popp, T., Poulson, C., Sawyer, V., Sogacheva, L., Thomas, G., Torres, O., Wang, Y., Kinne, S., Schulz, M., and Stier, P.: An AeroCom/AeroSat study: Intercomparison of Satellite AOD Datasets for Aerosol Model Evaluation, Atmos. Chem. Phys. Discuss., 2020, 1-43, 10.5194/acp-2019-1193, 2020.

Selden, T. M., and Song, D. Q.: Environmental Quality and Development - is there a Kuznets Curve for Air-Pollution Emissions?, Journal of Environmental Economics and Management, 27, 147-162, 10.1006/jeem.1994.1031, 1994.

Shah, V., Jacob, D. J., Li, K., Silvern, R. F., Zhai, S. X., Liu, M. Y., Lin, J. T., and Zhang, Q.: Effect of changing NOx lifetime on the seasonality and long-term trends of satellite-observed tropospheric NO2 columns over China, Atmospheric Chemistry and Physics, 20, 1483-1495, 10.5194/acp-20-1483-2020, 2020.

Shao, P. Y., Tian, H. Z., Sun, Y. J., Liu, H. J., Wu, B. B., Liu, S. H., Liu, X. Y., Wu, Y. M., Liang, W. Z., Wang, Y., Gao, J. J., Xue, Y. F., Bai, X. X., Liu, W., Lin, S. M., and Hu, G. Z.: Characterizing remarkable changes of severe haze events and chemical compositions in multi-size airborne particles (PM1, PM2.5 and PM10) from January 2013 to 2016-2017 winter in Beijing, China, Atmospheric Environment, 189, 133-144, 10.1016/j.atmosenv.2018.06.038, 2018.

584 Shi, X., and Brasseur, G. P.: The Response in Air Quality to the Reduction of Chinese Economic Activities during the
585 COVID-19 Outbreak, Geophysical Research Letters, 0-1, 10.1029/2020GL088070, 2020.

586 Si, Y. D., Wang, H. M., Cai, K., Chen, L. F., Zhou, Z. C., and Li, S. S.: Long-term (2006-2015) variations and relations
587 of multiple atmospheric pollutants based on multi-remote sensing data over the North China Plain, Environmental
588 Pollution, 255, 10.1016/j.envpol.2019.113323, 2019.

589 Sogacheva, L., Popp, T., Sayer, A. M., Dubovik, O., Garay, M. J., Heckel, A., Hsu, N. C., Jethva, H., Kahn, R. A.,
590 Kolmonen, P., Kosmale, M., de Leeuw, G., Levy, R. C., Litvinov, P., Lyapustin, A., North, P., Torres, O., and Arola,
591 A.: Merging regional and global aerosol optical depth records from major available satellite products, Atmospheric
592 Chemistry and Physics, 20, 2031-2056, 10.5194/acp-20-2031-2020, 2020.

593 Strode, S. A., Worden, H. M., Damon, M., Douglass, A. R., Duncan, B. N., Emmons, L. K., Lamarque, J.-F., Manyin,
594 M., Oman, L. D., Rodriguez, J. M., Strahan, S. E., and Tilmes, S.: Interpreting space-based trends in carbon monoxide
595 with multiple models, Atmospheric Chemistry and Physics, 16, 7285-7294, 10.5194/acp-16-7285-2016, 2016.

596 Sun, W., Shao, M., Granier, C., Liu, Y., Ye, C. S., and Zheng, J. Y.: Long-Term Trends of Anthropogenic SO2, NOx,
597 CO, and NMVOCs Emissions in China, Earths Future, 6, 1112-1133, 10.1029/2018ef000822, 2018.

598 United Nations Environment Program (UNEP): Independent Environmental Assessment: Beijing 2008 Olympic
599 Games. Nairobi, Kenya, 2009.

600 Wang, M., Zhu, T., Zheng, J., Zhang, R. Y., Zhang, S. Q., Xie, X. X., Han, Y. Q., and Li, Y.: Use of a mobile laboratory
601 to evaluate changes in on-road air pollutants during the Beijing 2008 Summer Olympics, Atmospheric Chemistry and
602 Physics, 9, 8247-8263, 10.5194/acp-9-8247-2009, 2009.

603 Wang, P., Chen, K., Zhu, S., Wang, P., and Zhang, H.: Severe air pollution events not avoided by reduced
604 anthropogenic activities during COVID-19 outbreak, Resources, Conservation and Recycling, 158, 104814,
605 10.1016/j.resconrec.2020.104814, 2020.

606 Wang, P. C., Elansky, N. F., Timofeev, Y. M., Wang, G. C., Golitsyn, G. S., Makarova, M. V., Rakitin, V. S., Shtabkin,
607 Y., Skorokhod, A. I., Grechko, E. I., Fokeeva, E. V., Safronov, A. N., Ran, L., and Wang, T.: Long-Term Trends of
608 Carbon Monoxide Total Columnar Amount in Urban Areas and Background Regions: Ground- and Satellite-based
609 Spectroscopic Measurements, Advances in Atmospheric Sciences, 35, 785-795, 10.1007/s00376-017-6327-8, 2018.

610 Wang, T., Nie, W., Gao, J., Xue, L. K., Gao, X. M., Wang, X. F., Qiu, J., Poon, C. N., Meinardi, S., Blake, D., Wang,
611 S. L., Ding, A. J., Chai, F. H., Zhang, Q. Z., and Wang, W. X.: Air quality during the 2008 Beijing Olympics:
612 secondary pollutants and regional impact, Atmospheric Chemistry and Physics, 10, 7603-7615, 10.5194/acp-10-7603-
613 2010, 2010.

614 Wang, Y., and Wang, J.: Tropospheric SO2 and NO2 in 2012-2018: Contrasting views of two sensors (OMI and
615 OMPS) from space, Atmospheric Environment, 223, 10.1016/j.atmosenv.2019.117214, 2020.

616 Warner, J., Carminati, F., Wei, Z., Lahoz, W., and Attie, J. L.: Tropospheric carbon monoxide variability from AIRS
617 under clear and cloudy conditions, Atmospheric Chemistry and Physics, 13, 12469-12479, 10.5194/acp-13-12469-
618 2013, 2013.

619 Witte, J. C., Schoeberl, M. R., Douglass, A. R., Gleason, J. F., Krotkov, N. A., Gille, J. C., Pickering, K. E., and
620 Livesey, N.: Satellite observations of changes in air quality during the 2008 Beijing Olympics and Paralympics,
621 Geophysical Research Letters, 36, 10.1029/2009gl039236, 2009.

Xie, G. Q., Wang, M., Pan, J., and Zhu, Y.: Spatio-temporal variations and trends of MODIS C6.1 Dark Target and Deep Blue merged aerosol optical depth over China during 2000-2017, Atmospheric Environment, 214, 10.1016/j.atmosenv.2019.116846, 2019.

Xu, J. H., Xie, H. M., Wang, K., Wang, J., and Xia, Z. S.: Analyzing the spatial and temporal variations in tropospheric NO2 column concentrations over China using multisource satellite remote sensing, Journal of Applied Remote Sensing, 14, 10.1117/1.jrs.14.014519, 2020.

Yu, S. M., Yuan, J. G., and Liang, X. Y.: Trends and Spatiotemporal Patterns of Tropospheric NO2 over China During 2005-2014, Water Air and Soil Pollution, 228, 10.1007/s11270-017-3641-9, 2017.

Yumimoto, K., Uno, I., and Itahashi, S.: Long-term inverse modeling of Chinese CO emission from satellite observations, Environmental Pollution, 195, 308-318, 10.1016/j.envpol.2014.07.026, 2014.

Zhang, Y., Li, C., Krotkov, N. A., Joiner, J., Fioletov, V., and McLinden, C.: Continuation of long-term global SO2 pollution monitoring from OMI to OMPS, Atmospheric Measurement Techniques, 10, 10.5194/amt-10-1495-2017, 2017.

Zhao, Y., Nielsen, C. P., McElroy, M. B., Zhang, L., and Zhang, J.: CO emissions in China: Uncertainties and implications of improved energy efficiency and emission control, Atmospheric Environment, 49, 103-113, 10.1016/j.atmosenv.2011.12.015, 2012.

Zhao, Y., Zhang, J., and Nielsen, C. P.: The effects of recent control policies on trends in emissions of anthropogenic atmospheric pollutants and CO2 in China, Atmospheric Chemistry and Physics, 13, 487-508, 10.5194/acp-13-487-2013, 2013.

Zheng, B., Chevallier, F., Ciais, P., Yin, Y., Deeter, M. N., Worden, H. M., Wang, Y. L., Zhang, Q., and He, K. B.: Rapid decline in carbon monoxide emissions and export from East Asia between years 2005 and 2016, Environmental Research Letters, 13, 10.1088/1748-9326/aab2b3, 2018a.

Zheng, B., Tong, D., Li, M., Liu, F., Hong, C. P., Geng, G. N., Li, H. Y., Li, X., Peng, L. Q., Qi, J., Yan, L., Zhang, Y. X., Zhao, H. Y., Zheng, Y. X., He, K. B., and Zhang, Q.: Trends in China's anthropogenic emissions since 2010 as the consequence of clean air actions, Atmospheric Chemistry and Physics, 18, 14095-14111, 10.5194/acp-18-14095-2018, 2018b.

Tables

Table 1. Summary statistics for central east China comparing 2020 and 2019 during January 23 – April 8.

Variable	2020 mean	2019 mean	2020 % difference from 2019
CO (ppbv)	133.5 (130.4, 136.8)	137.9 (134.6, 141.1)	-3 (-6, 0)
SO_2 (DU)	0.058 (0.045, 0.070)	0.031 (0.018, 0.046)	94 (16, 226)
NO_2 (10^{15} molec cm^{-2})	6.5 (5.8, 7.2)	9.6 (8.7, 10.5)	-32 (-41, -22)
AOD	0.41 (0.36, 0.46)	0.48 (0.41, 0.55)	-14 (-29, 3)

Table 2. Summary statistics for central east China during January 23 – April 8 over consistent trend periods. The background start year is that for which estimated trends explained most variability in the daily data through 2019, judging by the coefficient of determination (r^2) of the estimated trend. The background means and trends are estimated from the background start year through 2019, and the 2020 prediction is calculated from this trend. Numbers in parentheses are bootstrap-estimated 95% confidence intervals. The trends and percent differences are considered to be significant if their confidence intervals do not span 0.

Variable	Background start year	Background mean	2020 difference from background	trend (yr^{-1})	trend r^2	2020 predicted from trend	2020 % difference from trend
CO (ppbv)	2005	150.9 (149.8, 152.1)	-12 (-14, -9)	-1.8 (-2.0, -1.5)	0.17 (0.13, 0.21)	136.8 (134.8, 138.8)	-2 (-5, 1)
SO_2 (DU)	2012	0.206 (0.184, 0.231)	-72 (-79, -65)	-0.056 (-0.065, -0.047)	0.32 (0.26, 0.38)	-0.06 (-0.091, -0.032)	202 (159, 281)
NO_2 (10^{15} molec cm^{-2})	2011	11.3 (11.0, 11.7)	-43 (-49, -36)	-0.7 (-0.8, -0.5)	0.17 (0.11, 0.22)	7.8 (7.1, 8.5)	-17 (-28, -6)
AOD	2011	0.58 (0.55, 0.60)	-29 (-38, -19)	-0.03 (-0.04, -0.02)	0.08 (0.05, 0.12)	0.4 (0.36, 0.45)	2 (-15, 21)

661 **Table 3. Same as Table 1, but for southern China.**

Variable	2020 mean	2019 mean	2020 % difference from 2019
CO (ppbv)	144.9 (139.7, 150.3)	128.4 (124.3, 132.7)	13 (8, 18)
SO_2 (DU)	0.003 (-0.014, 0.020)	-0.023 (-0.039, -0.008)	122 (20, 217)
NO_2 (10^{15} molec cm^{-2})	3.3 (3.0, 3.7)	4.3 (3.8, 4.7)	-22 (-33, -10)
AOD	0.38 (0.34, 0.43)	0.34 (0.30, 0.39)	12 (-7, 33)

662

663 **Table 4. Same as Table 2, but for southern China.**

Variable	Background start year	Background mean	2020 difference from background	trend (yr^{-1})	trend r^2	2020 predicted from trend	2020 % difference from trend
CO (ppbv)	2016	137 (134.9, 139.1)	6 (2, 10)	-4.8 (-6.8, -3.0)	0.09 (0.03, 0.17)	125 (119.9, 130.4)	16 (10, 23)
SO_2 (DU)	2007	0.058 (0.048, 0.068)	-95 (-125, -65)	-0.012 (-0.015, -0.009)	0.13 (0.09, 0.17)	-0.034 (-0.050, -0.019)	109 (53, 165)
NO_2 (10^{15} molec cm^{-2})	2011	4.9 (4.7, 5.1)	-32 (-40, -24)	-0.3 (-0.3, -0.2)	0.08 (0.05, 0.13)	3.6 (3.2, 3.9)	-7 (-19, 8)
AOD	2011	0.46 (0.44, 0.48)	-17 (-27, -5)	-0.04 (-0.05, -0.03)	0.18 (0.12, 0.23)	0.28 (0.24, 0.31)	39 (15, 68)

664

665 **Table 5. 2014 anthropogenic emissions estimates by sector (in %) over China, excluding biomass burning, from the**
666 **Community Emissions Data System (CEDS) for a representative set of constituents: black carbon (BC), carbon monoxide**
667 **(CO), ammonia (NH_3), nitrogen oxides (NO_x), organic carbon (OC) and sulfur dioxide (SO_2). Residential, commercial and**
668 **other sectors are combined as RCO.**

	BC	CO	NH_3	NOx	OC	SO_2
Agriculture	0	0	61.6	1.1	0	0
Energy	32.6	8	0.4	38.5	28.3	29.4
Industrial	12.7	41.8	6.5	33	5.1	57.3
Ground transportation	8.1	7.2	0.5	17.5	1.7	0.3
RCO	38.1	36.7	5.2	4.2	38.4	12.5
Solvents	0	0	0	0	0	0
Waste	8.5	6.3	25.8	5.2	26.5	0.4
Shipping	0	0	0	0.2	0	0.1
Aircraft	0	0	0	0.2	0	0

669

Table 6. Bottom up biomass Global Fire Assimilation System (Kaiser et al., 2012) burning CO emissions estimates from the Upper Mekong region (17° N to 24° N, 95° E to 105° E) and AIRS CO over southern China from January 23 to April 8, for 2005-2020.

Year	GFAS CO Upper Mekong (KT)	AIRS CO southern China 500 hPa (ppbv)
2005	7977	157
2006	8905	146
2007	15734	165
2008	4542	153
2009	9990	140
2010	14176	149
2011	3591	147
2012	11320	153
2013	8684	145
2014	8722	142
2015	8084	143
2016	9642	149
2017	3736	131
2018	3179	139
2019	6309	128
2020	7871	145

Figures

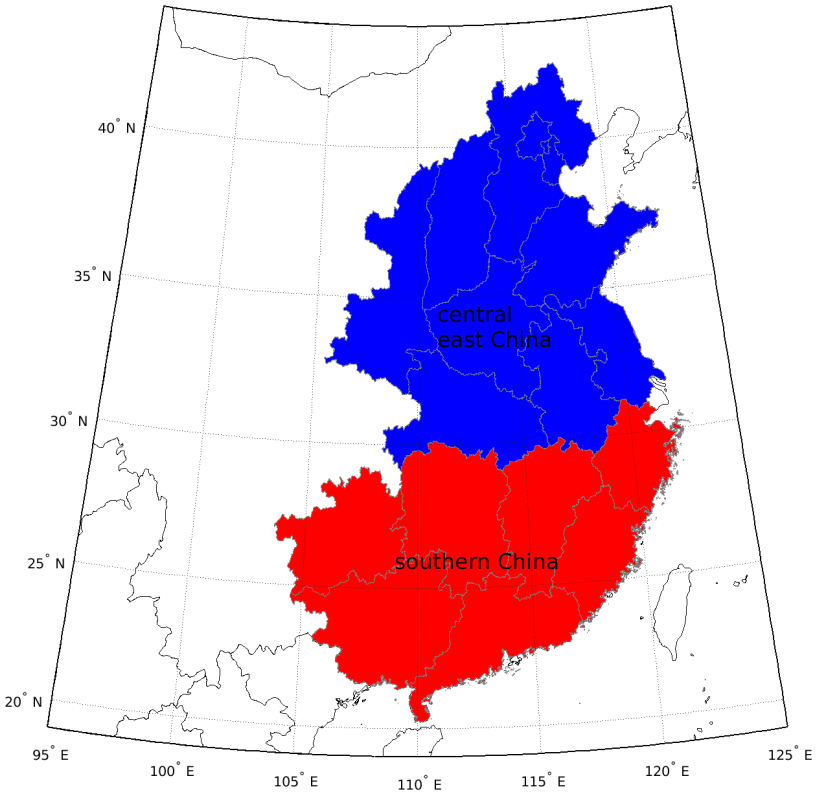

Figure 1. Groupings of provinces for central east China and southern China.

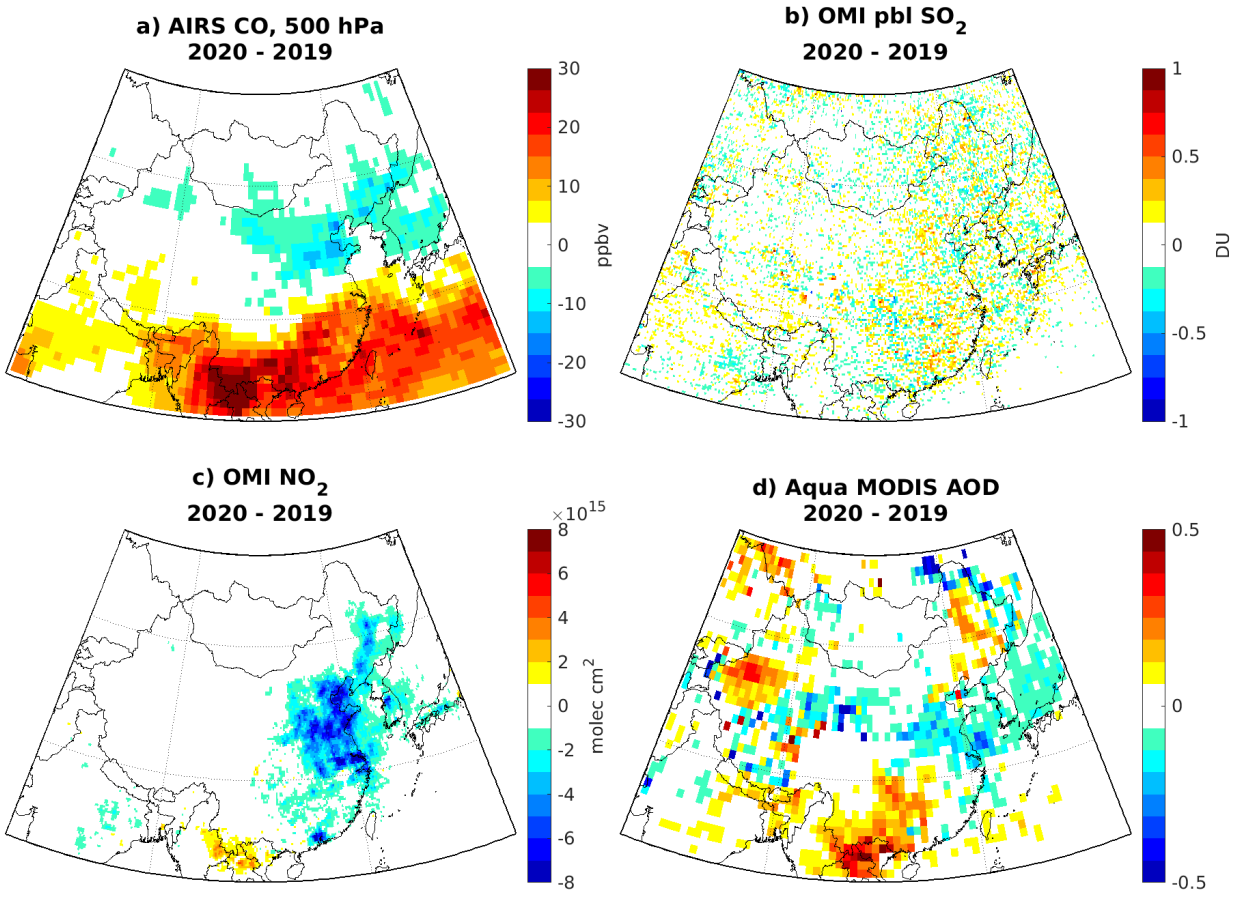

677

678 **Figure 2. 2020-2019 differences during January 23 to April 8 over China in a) AIRS carbon monoxide (CO) at 500 hPa, b)**
679 **OMI PBL sulfur dioxide (SO_2), c) OMI tropospheric nitrogen dioxide (NO_2) and d) Aqua MODIS aerosol optical depth**
680 **(AOD).**

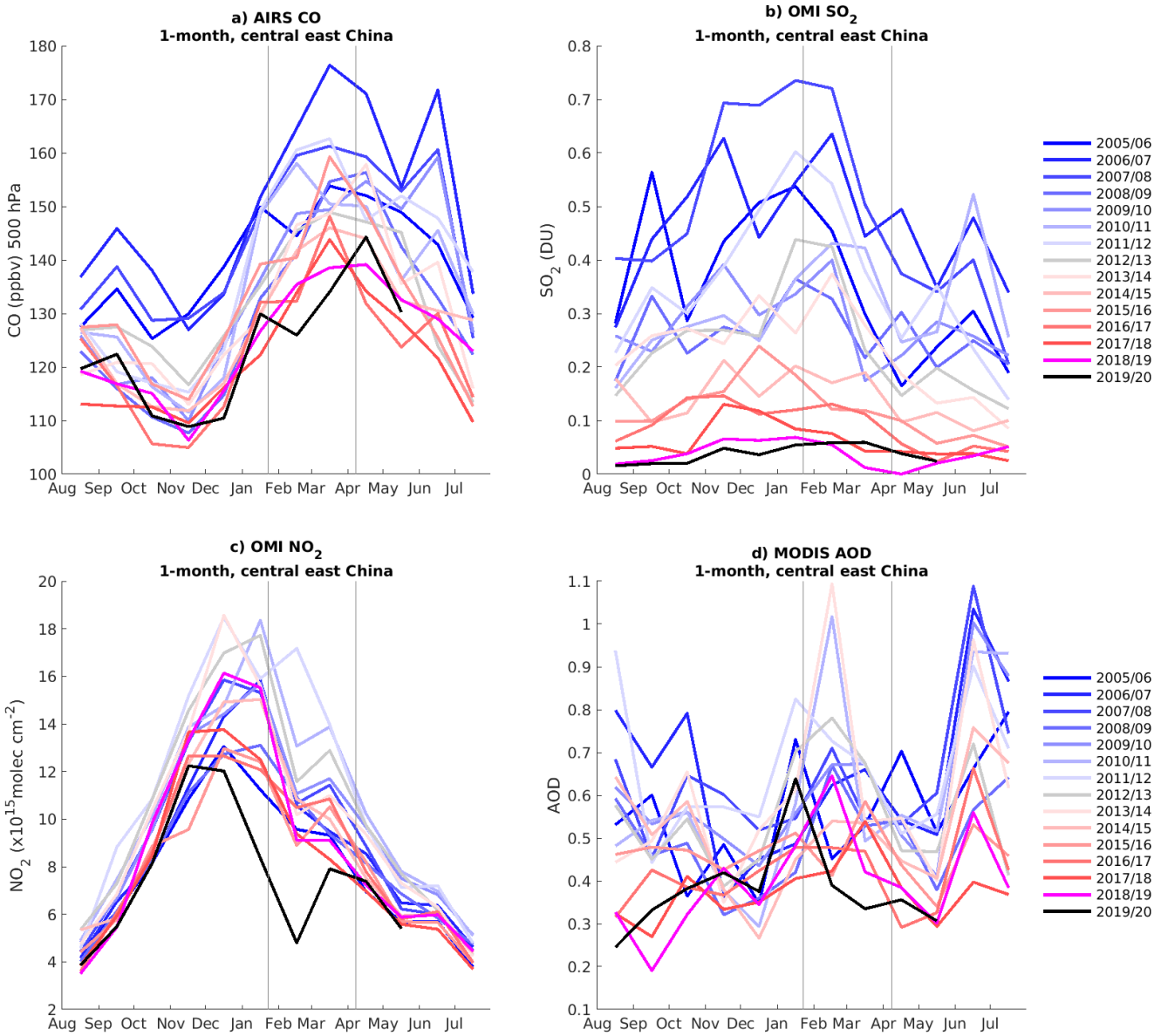

Figure 3. Monthly mean a) AIRS CO, b) OMI PBL SO_2, c) OMI tropospheric NO_2 and d) MODIS AOD over central east China since 2005. As in Bauwens et al. (2020), each year starts in August to show any departure from the seasonal cycle during the January 23 to April 8 lockdown period, shown by the thin grey vertical lines.

685

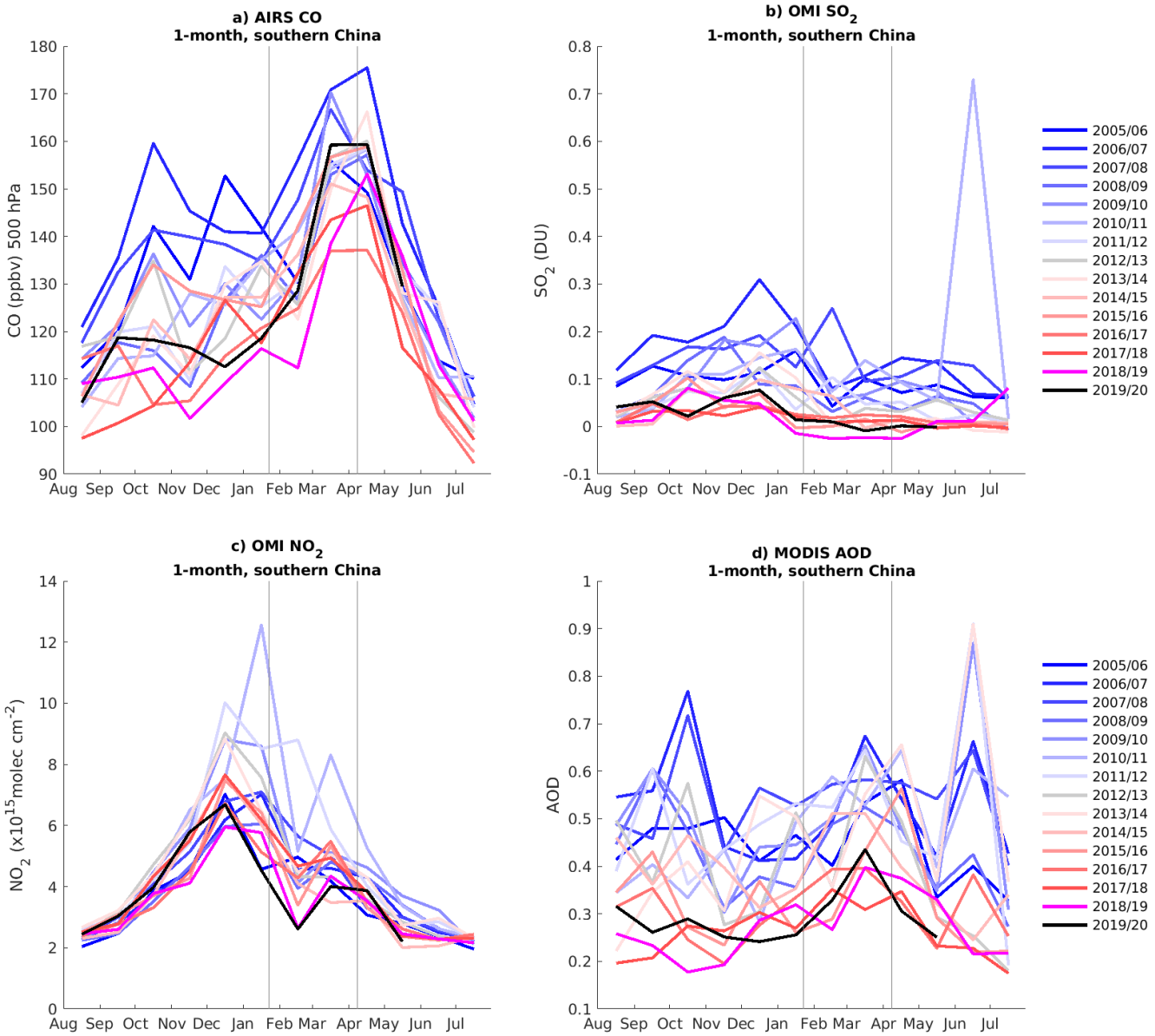

Figure 4. Same as Figure 3, but for southern China.

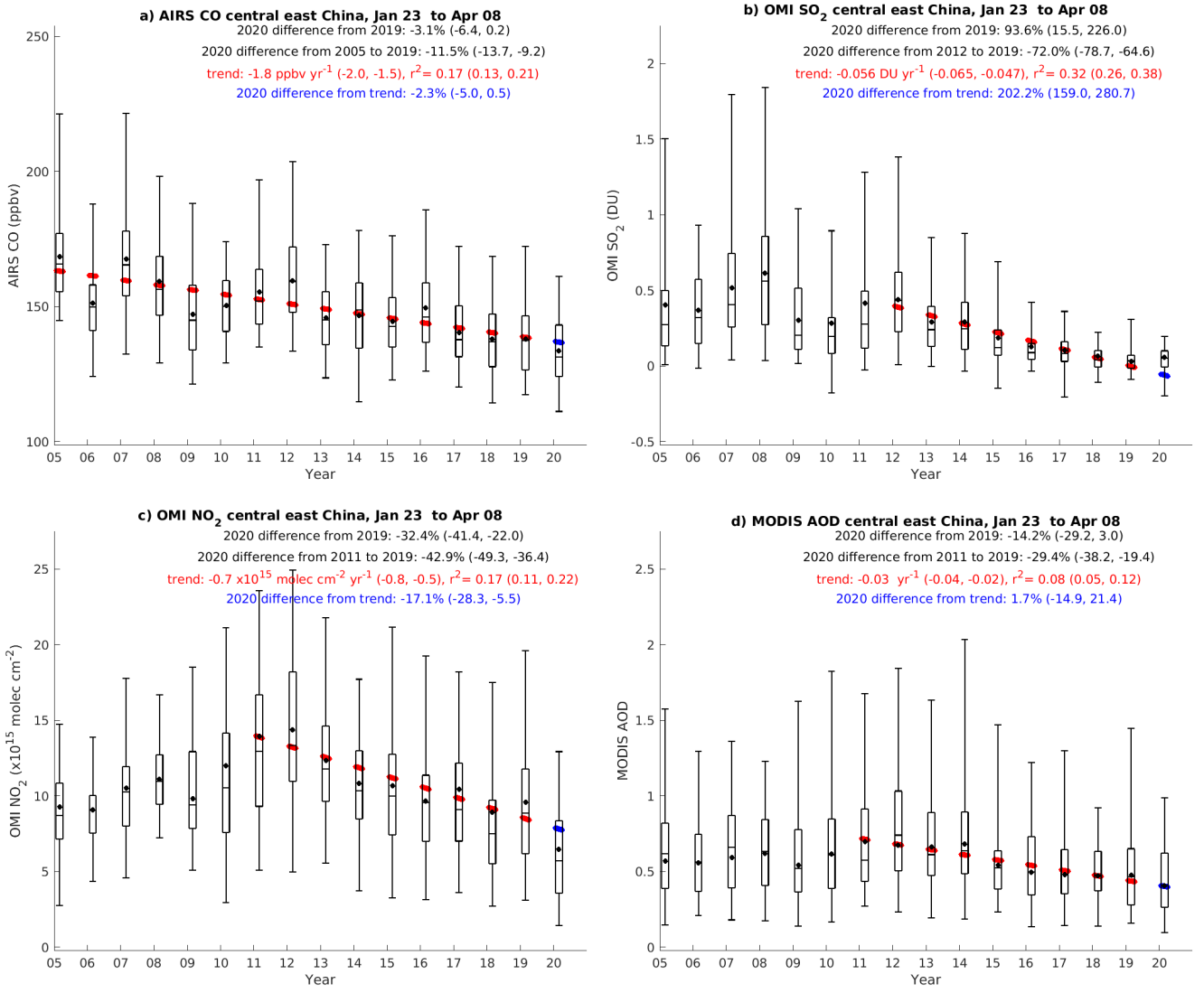

Figure 5. January 23-April 8 box plots over central East China for a) AIRS CO, b) OMI PBL SO_2, c) OMI tropospheric NO_2 and d) Aqua and Terra MODIS AOD from 2005 to 2020. The black box plots show the median, interquartile range and 2.5th and 97.5th percentiles over all daily data, with the mean shown by the black dot . For each variable, the estimated trend is plotted in red over the period during which it was strongest and given in the caption with its coefficient of determination (r^2). The percentage differences are given between 2020 and 2019, 2020 and the background period, and 2020 and the predicted value from the trend. 95% confidence intervals for each estimate are given in parentheses.

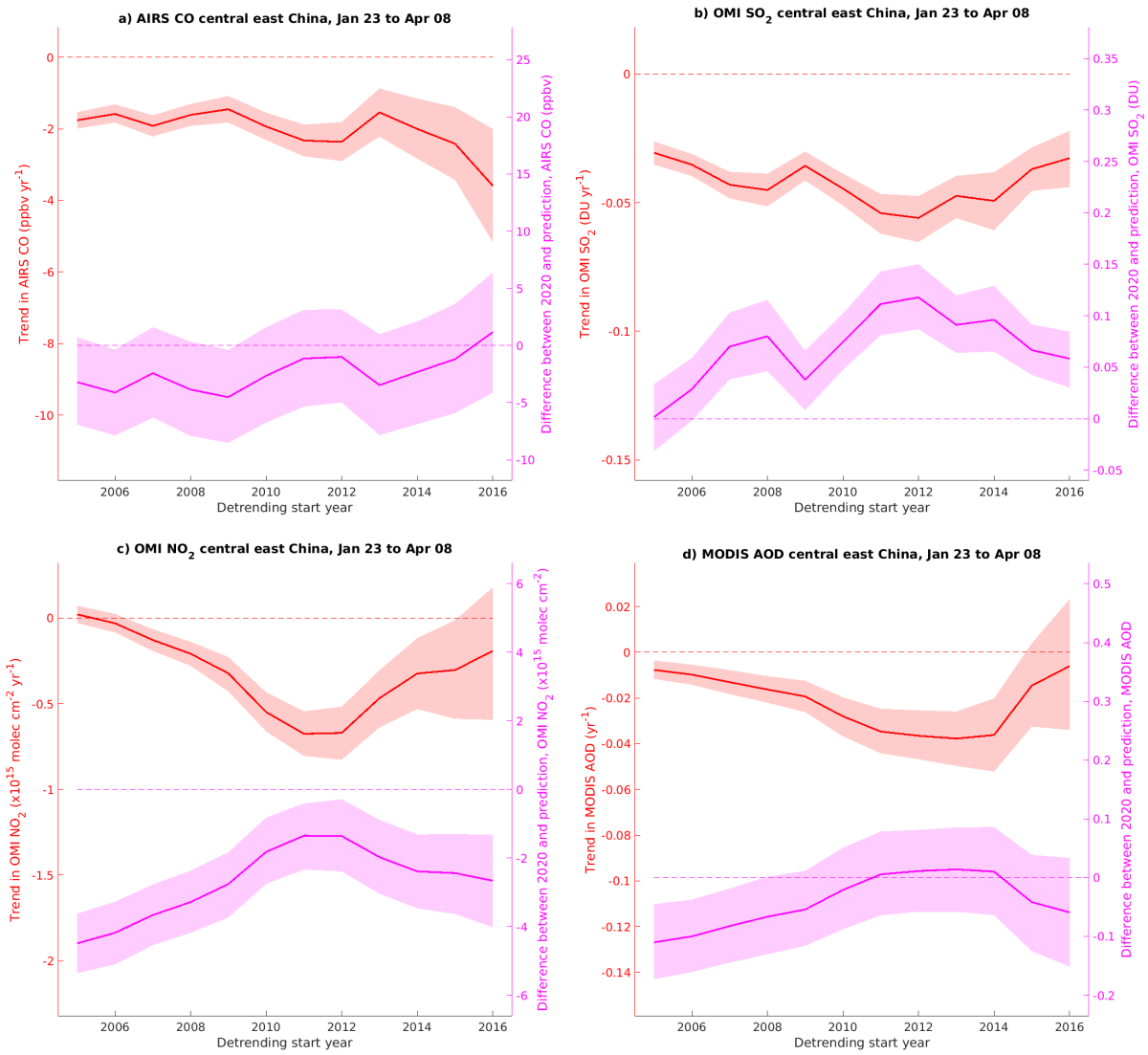

695

Figure 6. Dependence of trends (red) and difference between 2020 observations and predicted value (magenta) on detrending start year over central east China for a) AIRS CO, b) OMI PBL SO_2, c) OMI tropospheric NO_2 and d) MODIS AOD. The solid line shows the mean of the estimate for each year and the shading shows the 95% confidence interval.

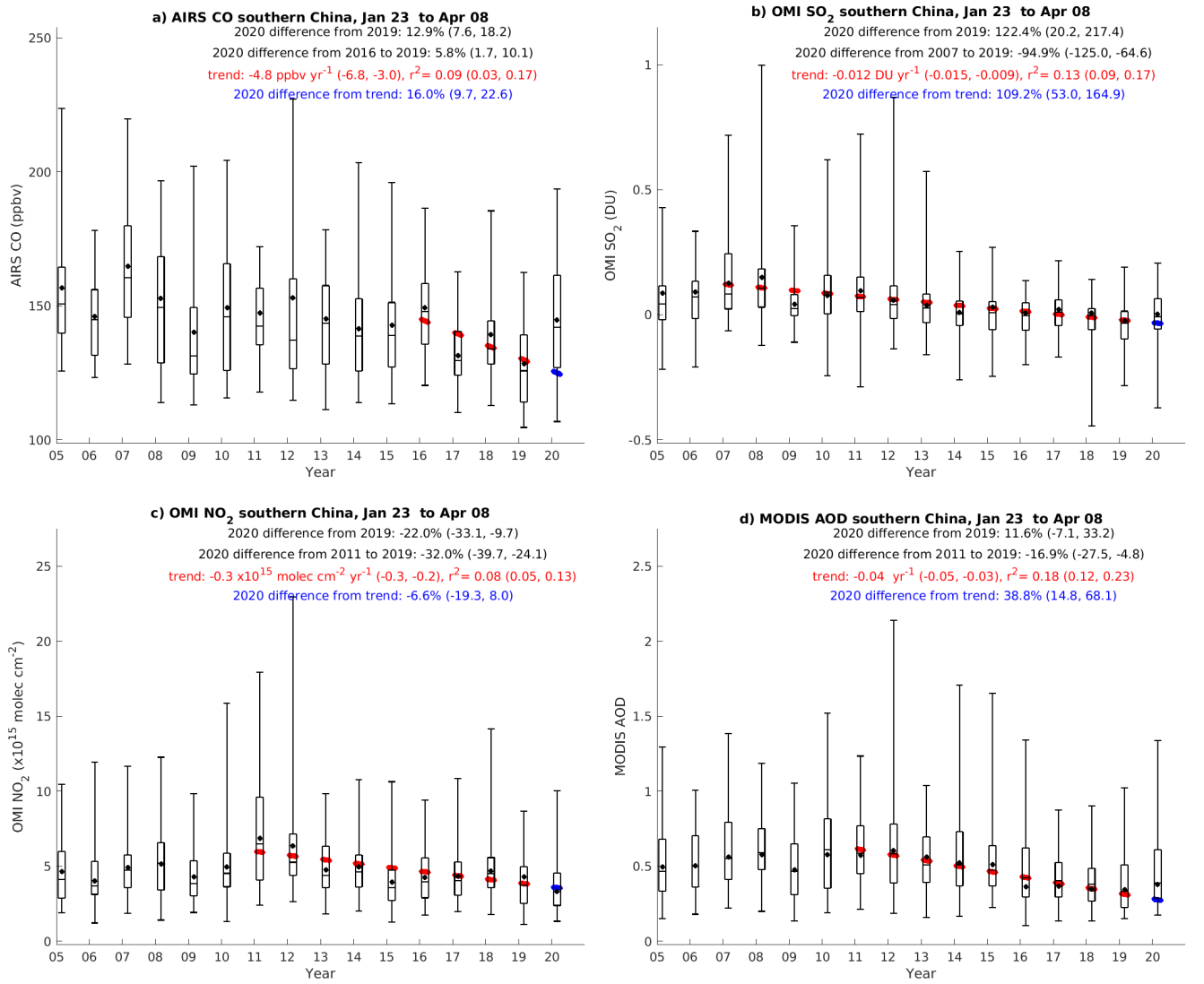

Figure 7. Same as Figure 5 but for southern China.

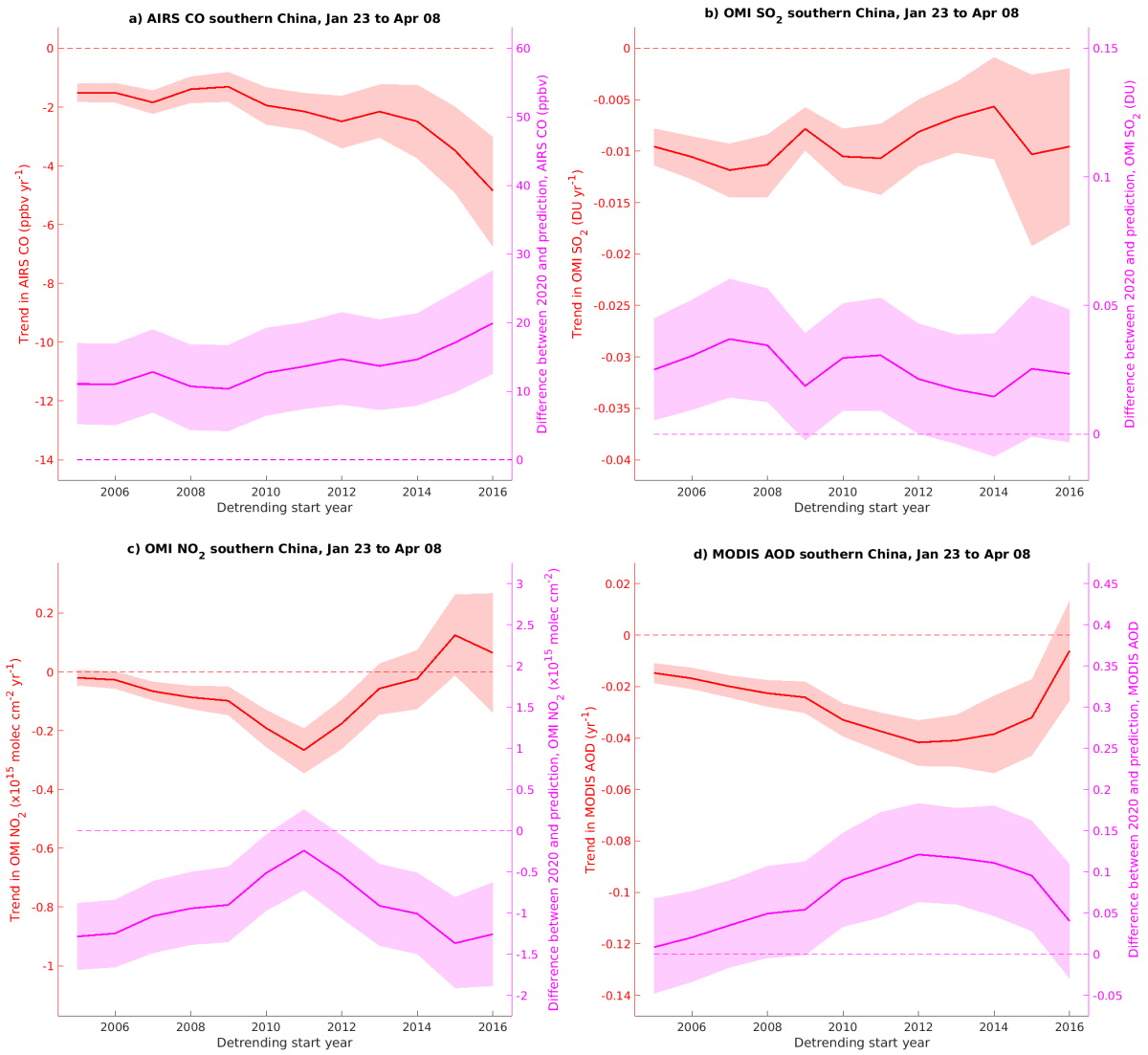

Figure 8. Same as Figure 6, but for southern China.